

Supporting Information

The Effect of Central and Planar Chirality on the Electrochemical and Chiral Sensing Properties of Ferrocenyl Urea H-Bonding Receptors

Andrea Mulas, Yasmine Willener, James Carr-Smith, Kevin M. Joly, Louise Male, Christopher J. Moody, Sarah L. Horswell, Huy V. Nguyen and James H.R. Tucker

Table of Contents

1.	Compound characterisation	Page S2
2.	X Ray crystal structures	Page S7
3.	NMR Binding studies	Page S13
4.	UV/vis binding studies	Page S20
5.	Electrochemistry	Page S21

1. Compound Characterisation

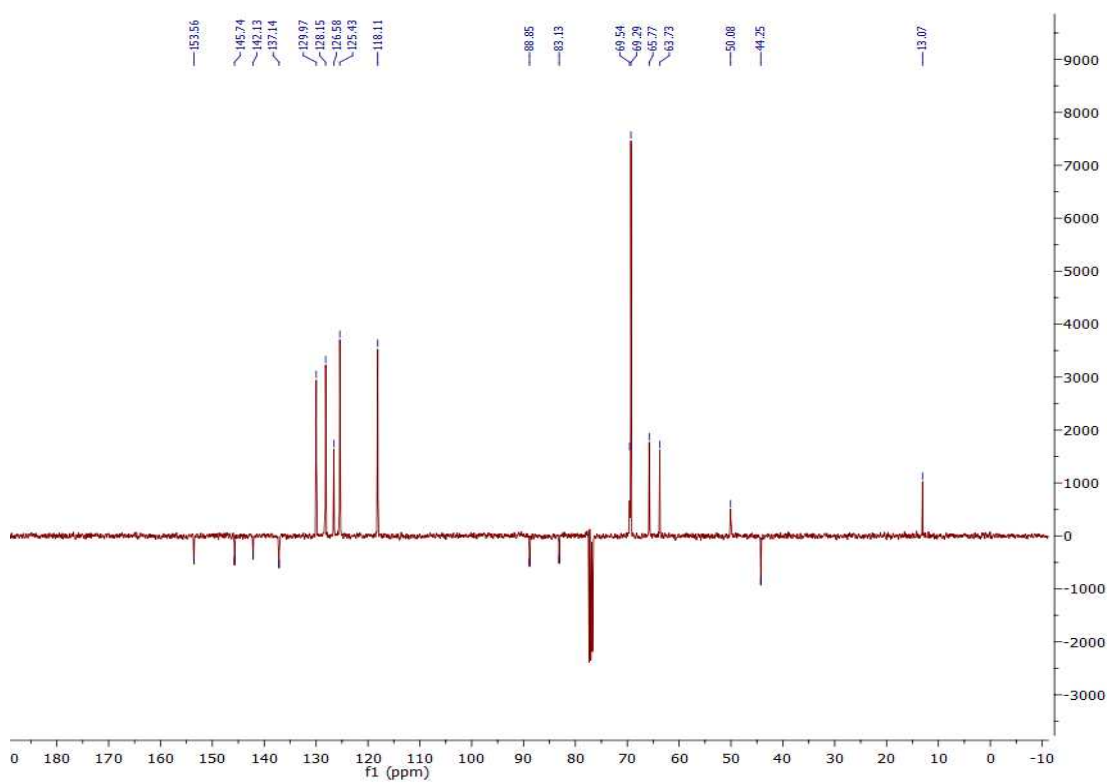
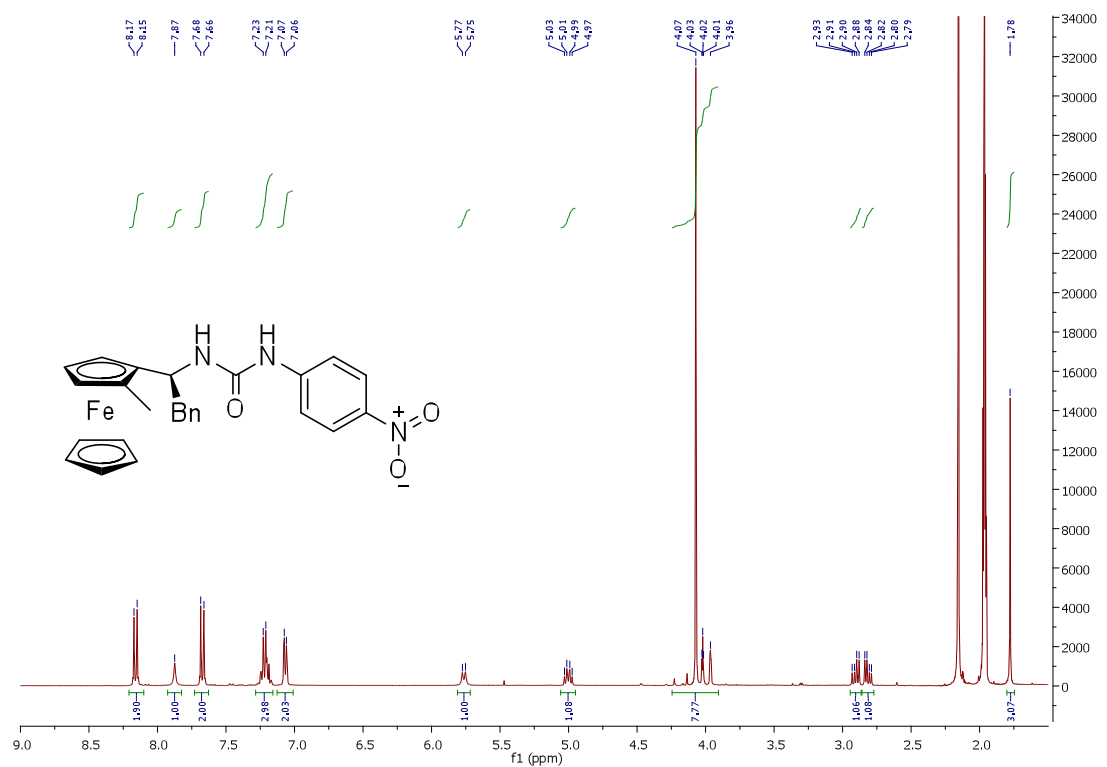


Figure S1 ¹H NMR and ¹³C (DEPT-135) spectrum of receptor **2** respectively in (CD₃)₂CO and CDCl₃.

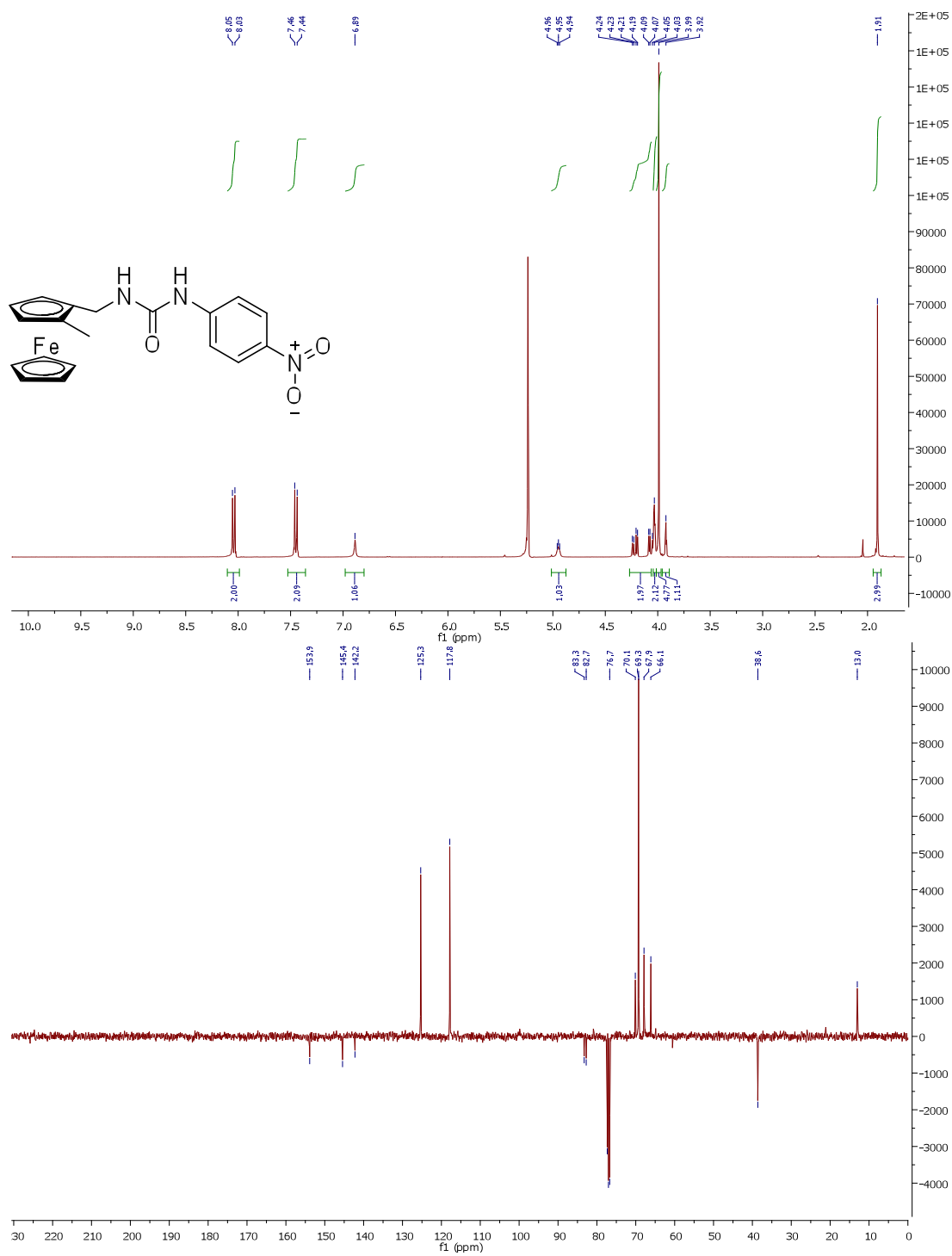


Figure S2 ¹H NMR and ¹³C (DEPT-135) NMR spectra of receptor (*R_p*)-**3** in CD₂Cl₂.

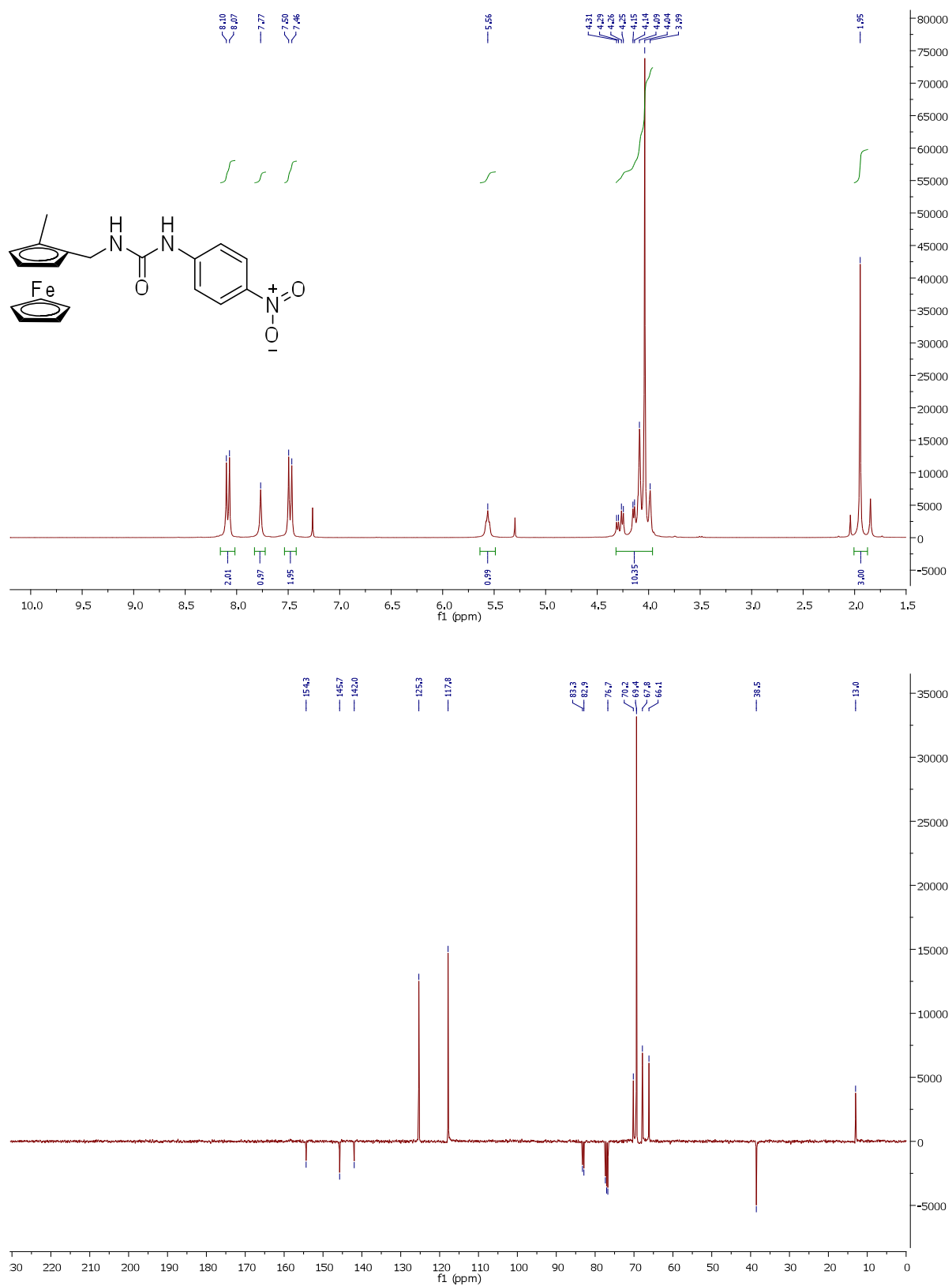


Figure S3 ¹H NMR and ¹³C (DEPT-135) NMR spectra of receptor (S_p)-3 in CDCl₃.

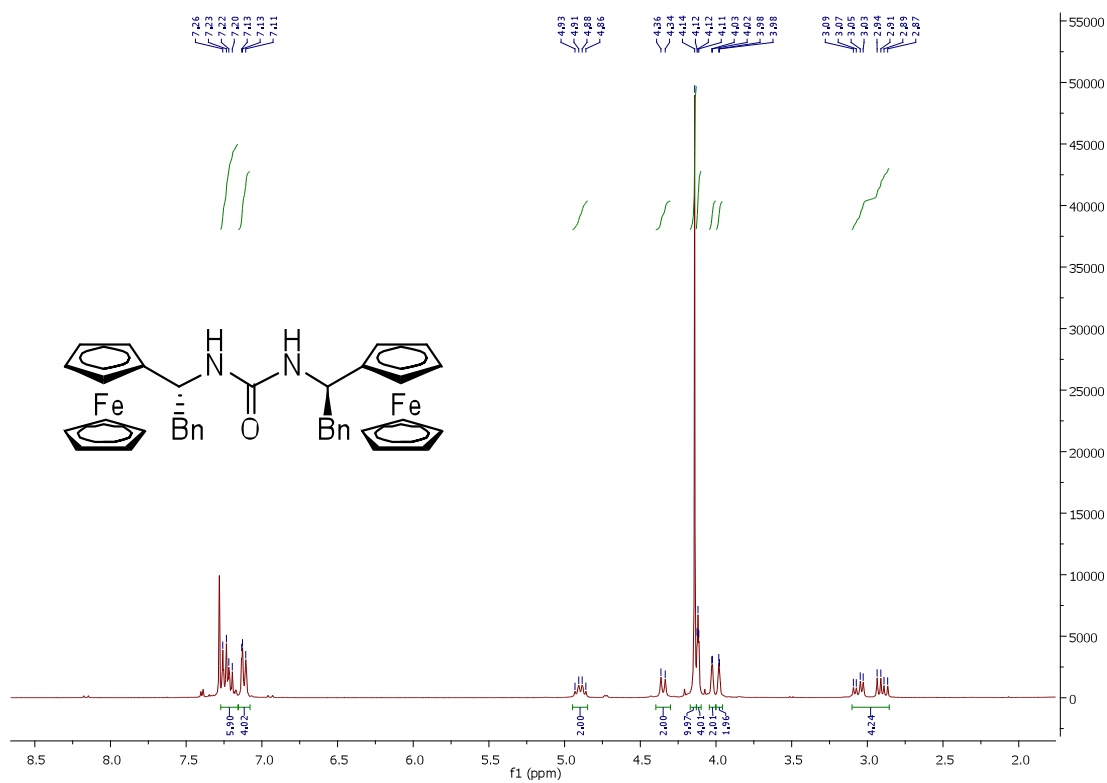
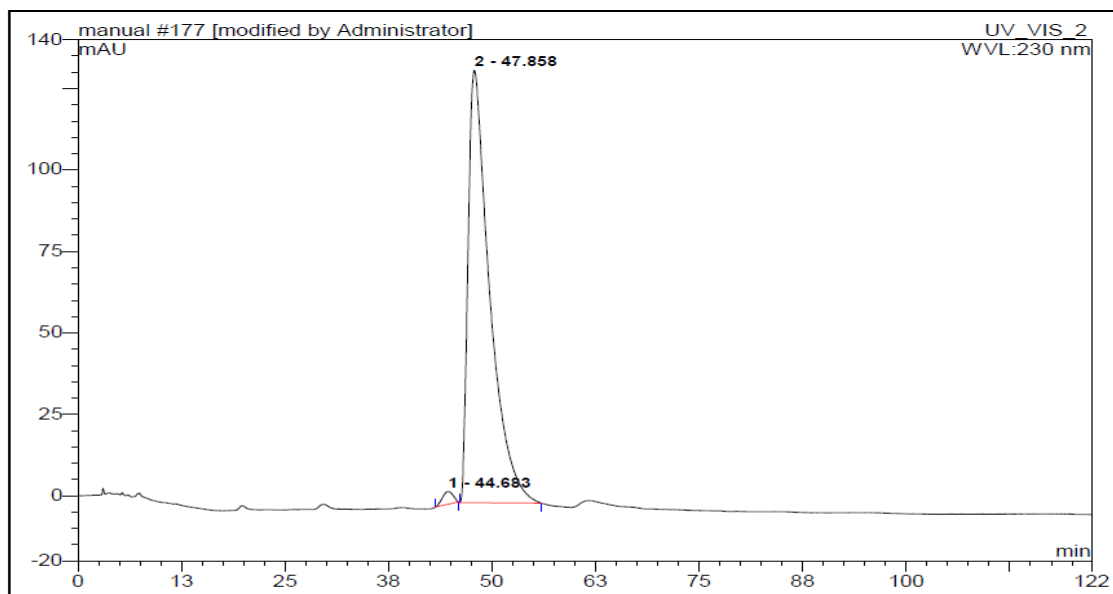
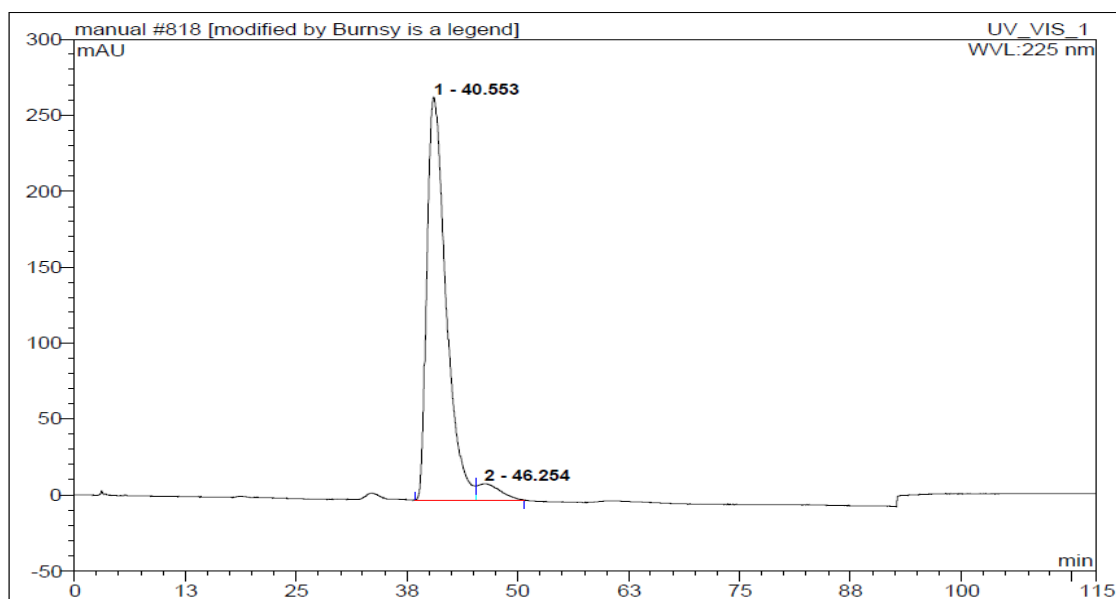


Figure S4 ¹H NMR spectrum of receptor **5** in CDCl₃



No.	Ret.Time min	Peak Name	Height mAU	Area mAU*min	Rel.Area %	Amount	Type
1	44.68	n.a.	3.927	5.867	1.45	n.a.	BMB*
2	47.86	n.a.	132.790	399.995	98.55	n.a.	BMB
Total:			136.717	405.862	100.00	0.000	



No.	Ret.Time min	Peak Name	Height mAU	Area mAU*min	Rel.Area %	Amount	Type
1	40.55	n.a.	265.312	661.326	95.37	n.a.	BM
2	46.25	n.a.	10.706	32.105	4.63	n.a.	MB
Total:			276.018	693.431	100.00	0.000	

Figure S5 Chiral HPLC of receptors (R_p)-3 (top) and (S_p)-3 (bottom) (10% IPA in hexane, AD column, 1 mL/min).

2. X-Ray Crystal Structures

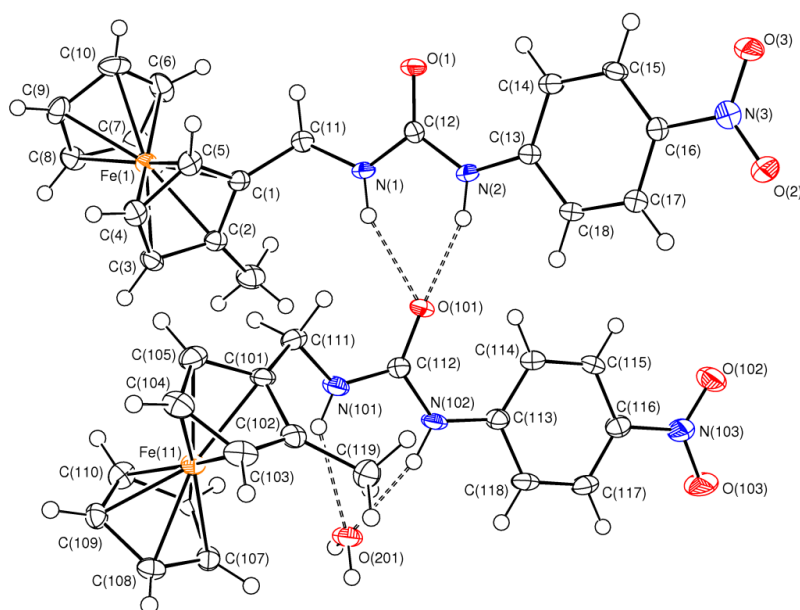


Figure S6 Crystal structure of the planar chiral receptor (R_p)-**3**·0.5H₂O, with ellipsoids drawn at 50% probability level. Dotted lines correspond to H-bonding. The structure contains two crystallographically-independent molecules and a water molecule is also included in the crystal. All hydrogen atoms are reported.

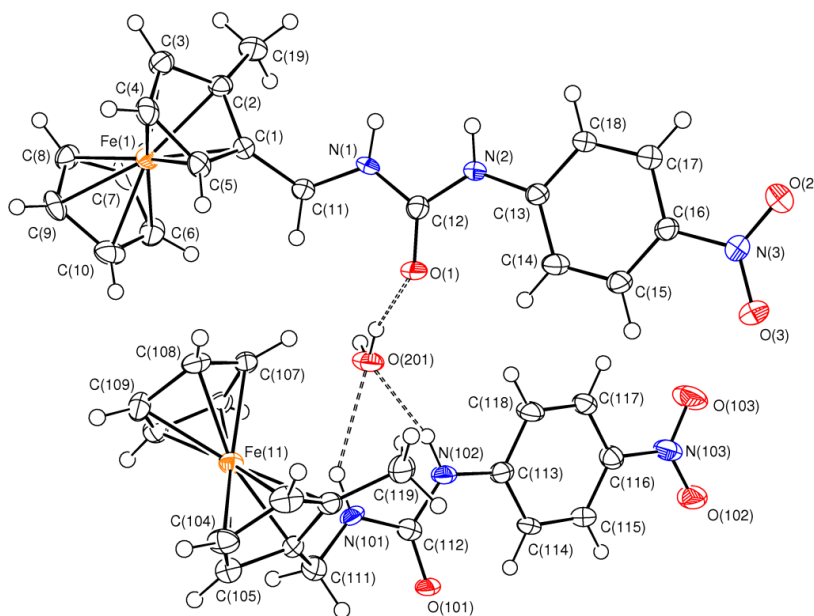


Figure S7 Crystal structure of the planar chiral receptor (S_p)-**3**·0.5H₂O, with ellipsoids drawn at 50% probability level. Dotted lines correspond to H-bonding. The structure contains two crystallographically-independent molecules and a water molecule is also included in the crystal. All hydrogen atoms are reported.

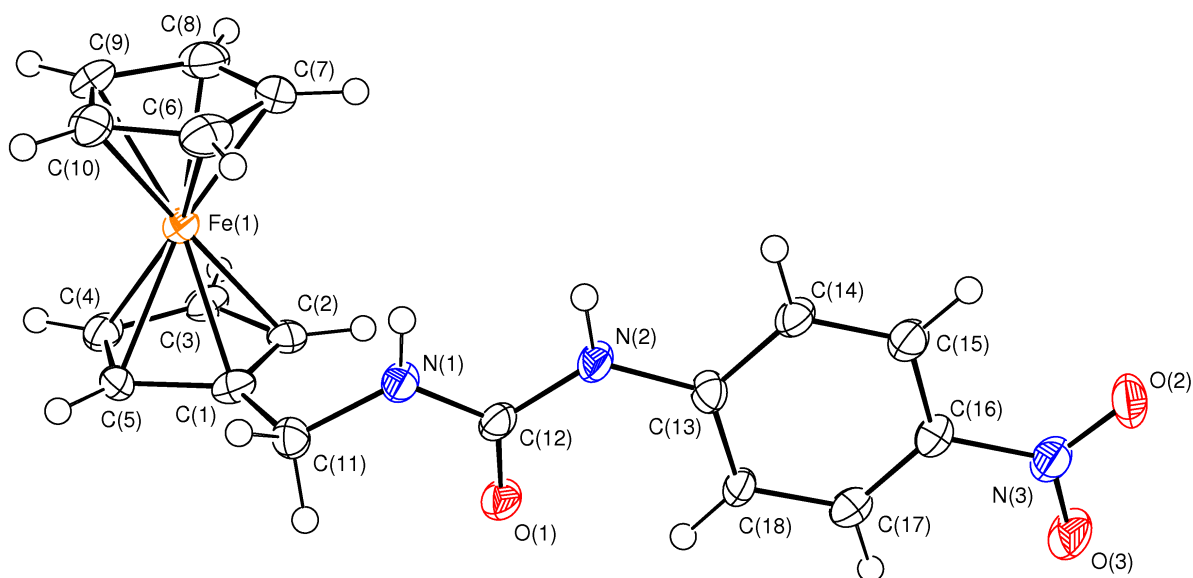


Figure S8 Crystal structure of the achiral receptor **4**, with ellipsoids drawn at 50% probability level. All hydrogen atoms are reported.

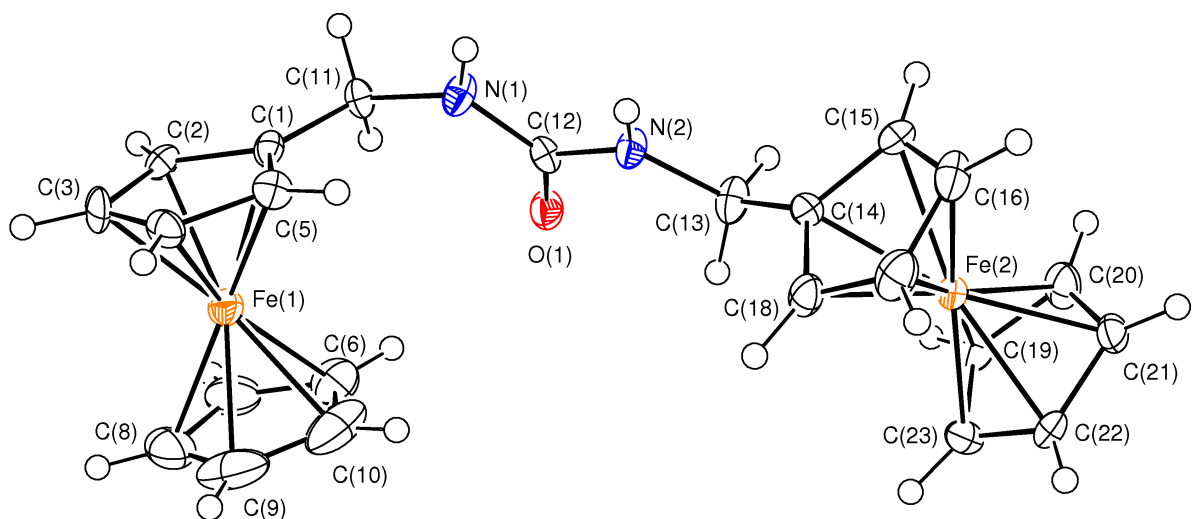


Figure S9 Crystal structure of the achiral receptor **6**, with ellipsoids drawn at 50% probability level. All hydrogen atoms are reported.

Table S1 Experimental data for compounds **3** - **6**.

	(<i>R</i> _p)- 3 ·0.5H ₂ O	(<i>S</i> _p)- 3 ·0.5H ₂ O	4	5 ·H ₂ O	6
Empirical Formula	C ₁₉ H ₁₉ FeN ₃ O ₃ , 0.5(H ₂ O)	C ₁₉ H ₁₉ FeN ₃ O ₃ , 0.5(H ₂ O)	C ₁₈ H ₁₇ FeN ₃ O ₃	C ₃₇ H ₃₆ Fe ₂ N ₂ O, H ₂ O	C ₂₃ H ₂₄ Fe ₂ N ₂ O
Formula Weight	402.23	402.23	379.20	654.39	456.14
Temperature (K)	120 (2)	120 (2)	120 (2)	120 (2)	120 (2)
Crystal System	Monoclinic	Monoclinic	Monoclinic	Orthorhombic	Orthorhombic
Space Group	<i>P</i> 2 ₁	<i>P</i> 2 ₁	<i>Cc</i>	<i>P</i> 2 ₁ 2 ₁ 2 ₁	<i>P</i> 2 ₁ 2 ₁ 2 ₁
<i>a</i> ; <i>b</i> ; <i>c</i> (Å)	11.1740(3) ; 7.2448(2) ; 22.0107(6)	11.1747(5) ; 7.2439(3) ; 22.0137(11)	5.7835(4) ; 30.636(3) ; 9.2241(8)	6.2750(2) ; 19.7316(7) ; 24.4396(8)	8.5102(4) ; 8.7702(5) ; 26.0912(15)
<i>β</i> (°)	92.120(1)	92.116(2)	96.405(6)	90	90
<i>V</i> (Å ³)	1780.62(8)	1780.76(14)	1624.2(2)	3026.01(18)	1947.35(18)
<i>Z</i> ; <i>Z'</i>	4 ; 2	4 ; 2	4 ; 1	4 ; 1	4 ; 1
Reflections Collected	19184	22029	8429	26247	13280
Independent Reflections	7983 [<i>R</i> _{int} = 0.0464]	7713 [<i>R</i> _{int} = 0.0752]	2707 [<i>R</i> _{int} = 0.0445]	5342 [<i>R</i> _{int} = 0.0912]	4389 [<i>R</i> _{int} = 0.0656]
<i>θ</i> Range for Data Collection (°)	2.96 – 27.48	2.96 – 27.48	3.47 - 25.03	3.21 - 25.02	3.12 – 27.48
Completeness to <i>θ</i> _{max}	99.6	99.4	99.6	99.8	99.4
Goodness-of-Fit on <i>F</i> ²	1.040	1.014	1.067	1.043	1.169
Final <i>R</i> Indices (Observed Data)	<i>R</i> 1 = 0.0434, <i>wR</i> 2 = 0.0880	<i>R</i> 1 = 0.0542, <i>wR</i> 2 = 0.0998	<i>R</i> 1 = 0.0374, <i>wR</i> 2 = 0.0783	<i>R</i> 1 = 0.0499, <i>wR</i> 2 = 0.0736	<i>R</i> 1 = 0.0671, <i>wR</i> 2 = 0.1164
Final <i>R</i> Indices (All Data)	<i>R</i> 1 = 0.0555, <i>wR</i> 2 = 0.0933	<i>R</i> 1 = 0.0863, <i>wR</i> 2 = 0.1118	<i>R</i> 1 = 0.0419, <i>wR</i> 2 = 0.0811	<i>R</i> 1 = 0.0752, <i>wR</i> 2 = 0.0792	<i>R</i> 1 = 0.0932, <i>wR</i> 2 = 0.1287
Largest Diff. Peak ; Hole (e Å ⁻³)	0.383; -0.559	0.410 ; -0.485	0.265 ; -0.345	0.372 ; -0.305	0.521 ; -0.521
Flack Parameter	0.036(13)	0.056(17)	0.13(2)	0.050(19)	0.16(4)
CCDC	950562	950563	950564	950565	950566

Suitable crystals were selected and datasets were measured by the EPSRC UK National Crystallography Service¹ on a Bruker KappaCCD diffractometer for (*R*_p)-**3**·0.5H₂O, (*S*_p)-**3**·0.5H₂O and **5**·H₂O and on a Bruker APEXII CCD diffractometer for **4** and **6**, both at the window of a Bruker FR591 rotating anode ($\lambda_{\text{Mo-K}\alpha} = 0.71073 \text{ \AA}$). The data collections were driven by COLLECT² and were processed by DENZO³ and absorption corrections were applied using SADABS.⁴ The structures were solved using ShelXS-97⁵ and refined by a full-matrix least-squares procedure on F² in ShelXL-97.⁵ All non-hydrogen atoms were refined with anisotropic displacement parameters. The water-bound hydrogen atoms in (*R*_p)-**3**·0.5H₂O, (*S*_p)-**3**·0.5H₂O and **5**·H₂O were located in the electron density and the positions refined subject to O-H and H...H distance restraints (0.88(2) Å and 1.41(4) Å respectively). All remaining hydrogen atoms were added at calculated positions and refined by use of a riding model. With the exception of the water-bound hydrogen atoms in (*R*_p)-**3**·0.5H₂O the isotropic displacement parameters for all hydrogen atoms were based on the equivalent isotropic displacement parameter (*U*_{eq}) of the parent atom. Figures were produced using ORTEP-3 for Windows.⁶

- 1 P. A. Gale and S. J. Coles, *Chem. Sci.*, 2012, **3**, 683-689.
- 2 R. W. W. Hooft, 1998, *COLLECT Data Collection Software*, Nonius B. V., Delft.
- 3 Z. Otwinowski and W. Minor, in *Methods in Enzymology*, ed. C. W. Carter and R. M. Sweet, Academic Press, New York, 1997, vol. 276, pp. 307-326.
- 4 G. M. Sheldrick, 2007, *SADABS*, Bruker AXS Inc., Madison, Wisconsin, USA.
- 5 G. M. Sheldrick, *Acta Cryst.*, 2008, **A64**, 112-122.
- 6 L. J. Farrugia, *J. Appl. Cryst.*, 1997, **30**, 565.

Table S2 Selected bond lengths (Å) and angles (°) for **3** – **6**.

	<i>(R_p)</i> - 3 ·0.5H ₂ O	<i>(S_p)</i> - 3 ·0.5H ₂ O	4	5 ·H ₂ O	6
3, 4, 6: C(11)-N(1) / C(111)-N(101) 5 ·H ₂ O: C(21)-N(1)	1.465(4) / 1.457(4)	1.464(5) / 1.460(5)	1.460(5)	1.465(5)	1.443(6)
3, 4, 6: N(1)-C(12) / N(101)-C(112) 5 ·H ₂ O: N(1)-C(22)	1.345(4) / 1.344(4)	1.346(5) / 1.350(5)	1.344(5)	1.361(4)	1.358(7)
3, 4, 6: C(12)-O(1) / C(112)-O(101) 5 ·H ₂ O: C(22)-O(1)	1.237(3) / 1.236(3)	1.227(4) / 1.234(5)	1.217(5)	1.246(4)	1.248(6)
3, 4, 6: C(12)-N(2) / C(112)-N(102) 5 ·H ₂ O: C(22)-N(2)	1.381(4) / 1.376(4)	1.385(5) / 1.374(6)	1.400(5)	1.358(5)	1.352(7)
3, 4, 6: N(2)-C(13) / N(102)-C(113) 5 ·H ₂ O: N(2)-C(23)	1.395(4) / 1.392(4)	1.390(5) / 1.391(6)	1.404(5)	1.454(4)	1.455(7)
3, 4, 6: C(11)-N(1)-C(12) / C(111)-N(101)-C(112) 5 ·H ₂ O: C(21)-N(1)-C(22)	124.3(2) / 122.2(2)	124.0(3) / 121.9(3)	121.1(3)	123.1(3)	124.0(5)
3, 4, 6: N(1)-C(12)-O(1) / N(101)-C(112)-O(101) 5 ·H ₂ O: N(1)-C(22)-O(1)	124.4(3) / 123.0(3)	124.9(4) / 123.2(4)	124.0(4)	121.7(4)	122.7(5)
3, 4, 6: O(1)-C(12)-N(2) / O(101)-C(112)-N(102) 5 ·H ₂ O: O(1)-C(22)-N(2)	123.2(3) / 123.1(3)	123.3(4) / 122.9(4)	122.9(3)	124.3(4)	121.9(5)
3, 4, 6: N(1)-C(12)-N(2) / N(101)-C(112)-N(102) 5 ·H ₂ O: N(1)-C(22)-N(2)	112.4 (2) / 113.9(2)	111.8 (3) / 113.9(4)	113.1(3)	114.0(4)	115.4(5)
3, 4, 6: C(12)-N(2)-C(13) / C(112)-N(102)-C(113) 5 ·H ₂ O: C(22)-N(2)-C(23)	130.5(3) / 128.1(2)	130.2(3) / 128.2(4)	127.0(3)	123.7(3)	121.7(5)

Table S3 Intermolecular hydrogen bond lengths (Å) and angles (°) for **3** – **6**.

	D-H...A	d(D-H)	d(H...A)	d(D...A)	<(DHA)
<i>(R_p)</i> - 3 ·0.5H ₂ O	N(1)-H(1)...O(101)	0.88	2.09	2.907(3)	153.4
	N(2)-H(2)...O(101)	0.88	1.98	2.824(3)	161.2
	N(101)-H(101)...O(201)	0.88	2.38	3.133(3)	144.0
	N(102)-H(102)...O(201)	0.88	1.95	2.811(3)	165.4
	O(201)-H(21A)...O(102)#1	0.882(18)	2.49(3)	3.122(4)	129(3)
	O(201)-H(21B)...O(1)#2	0.889(18)	1.85(2)	2.724(3)	167(4)
<i>(S_p)</i> - 3 ·0.5H ₂ O	N(1)-H(1)...O(101)#3	0.88	2.10	2.911(4)	153.8
	N(2)-H(2)...O(101)#3	0.88	1.98	2.827(4)	161.5
	N(101)-H(101)...O(201)	0.88	2.38	3.136(5)	143.6
	N(102)-H(102)...O(201)	0.88	1.96	2.818(4)	166.0
	O(201)-H(21A)...O(1)	0.871(19)	1.87(2)	2.720(4)	164(5)
	O(201)-H(21B)...O(102)#4	0.876(19)	2.42(3)	3.122(5)	137(4)
4	N(1)-H(1A)...O(2)#5	0.88	2.29	3.096(4)	151.4
	N(2)-H(2A)...O(2)#5	0.88	2.18	3.021(4)	159.4
5 ·H ₂ O	N(1)-H(1)...O(101)	0.88	2.08	2.884(4)	151.8
	N(2)-H(2A)...O(101)	0.88	2.06	2.860(4)	149.9
	O(101)-H(01A)...O(1)#6	0.862(18)	1.787(19)	2.643(4)	172(4)
6	N(1)-H(1A)...O(1)#7	0.88	2.16	2.959(6)	150.8
	N(2)-H(2A)...O(1)#7	0.88	2.08	2.880(6)	150.2

Symmetry transformations used to generate equivalent atoms:

#1 -x+1,y-1/2,-z+1; #2 x-1,y,z; #3 x+1,y,z; #4 -x,y+1/2,-z; #5 x-1,-y,z+1/2; #6 x+1,y,z; #7 -x,y-1/2,-z+1/2

3. NMR Binding Studies

NMR Titrations NMR measurements were performed at 300 MHz on a Bruker AVIII300 NMR spectrometer and at 400 MHz on a Bruker AV400 NMR spectrometer. The receptor (5 mM) was titrated with a solution of the guest (50 mM) dissolved in the stock solution of the host, to avoid dilution effects. After each addition of guest solution, a ¹H NMR spectrum was recorded and signals corresponding to the urea protons were noted. The binding constant values, *K*, were determined from the titrations data, using the WinEqNMR software.¹⁷⁻¹⁸

Job Plots Solutions of the host and the guest were prepared (5 mM) in the appropriate solvent (e.g. CD₃CN or 2:1 CD₃CN/CD₂Cl₂). These solutions were then combined with the following host:guest ratio (in μ l): 500:0, 450:50, 400:100, 350:150, 300:200, 250:250, 200:300, 150:350, 100:400 and 50:450. A ¹H NMR experiment was recorded of each resulting solution, and shift of significant peaks upon complexation was observed. The concentration of the complex formed was calculated using the data obtained through Equation S1 and then plotted against the mole fraction of host.

$$[complex]_{r:500-n} = [H]_{n:500-n} \left(\frac{\delta_{obs} - \delta_0}{\delta_{comp} - \delta_0} \right) \quad \text{Equation S1}$$

where:

n = volume of host (μ l)

$[H]$ = concentration of host in solution (mM)

δ_{obs} = observed shift of the proton resonance monitored

δ_0 = shift of the proton resonance observed for the host in absence of substrate

δ_{comp} = shift of the proton resonance observed for the host upon full complexation

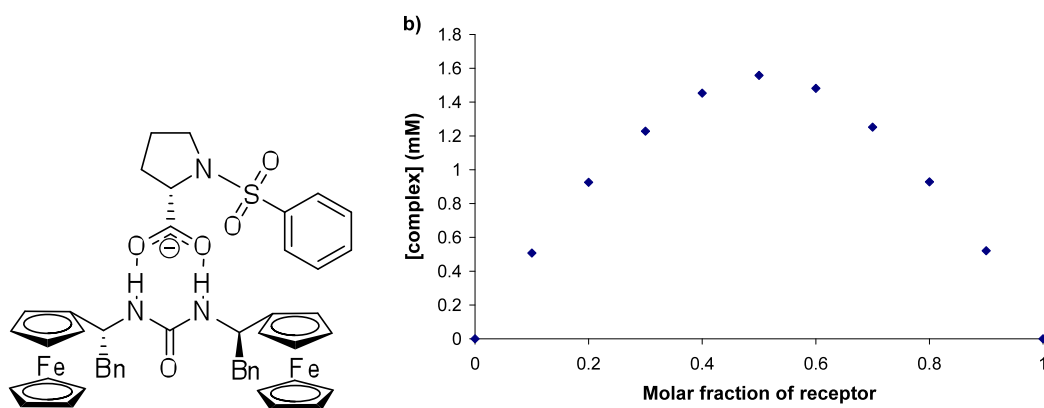


Figure S10 Structure of the 1:1 complex between the chiral host **5** and the guest *(S)*-**9** in CD₃CN, as indicated by a Job Plot with a maximum complex concentration at a mole fraction of 0.5.

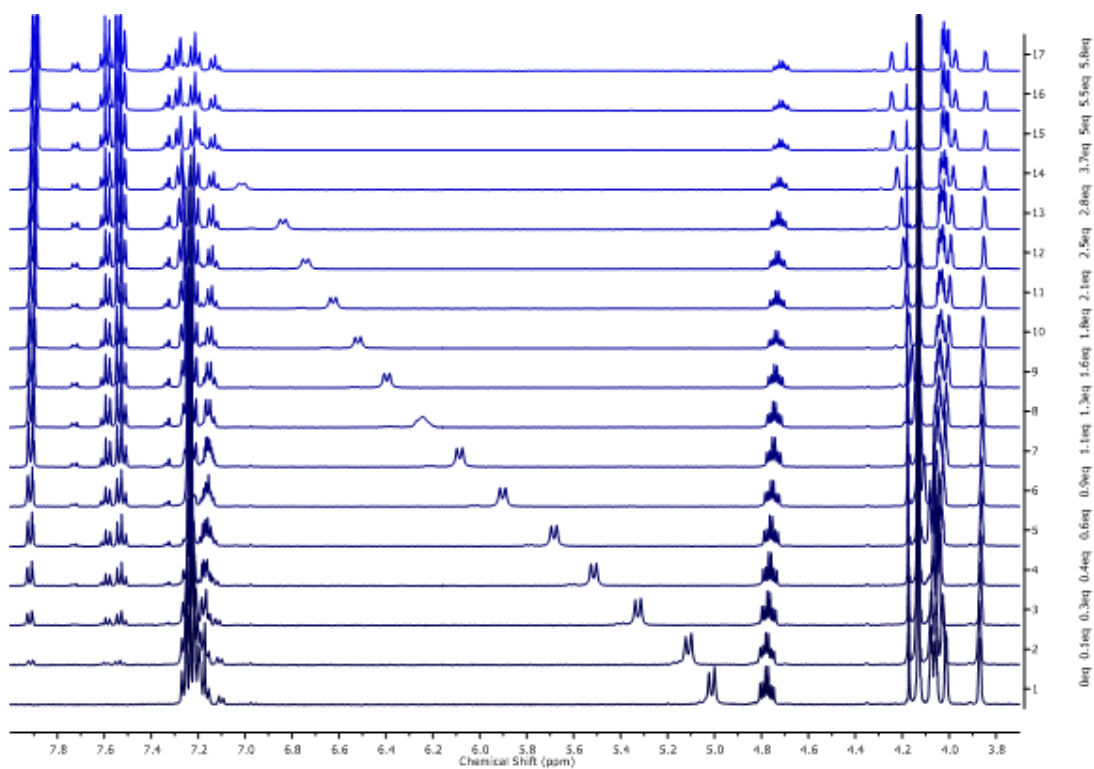


Figure S11 Stacked ^1H NMR Spectra for the titration of **5** (5 mM) with (*R*)-**9** (50 mM) in CD_3CN at rt (addition of up to 6 equivalents).

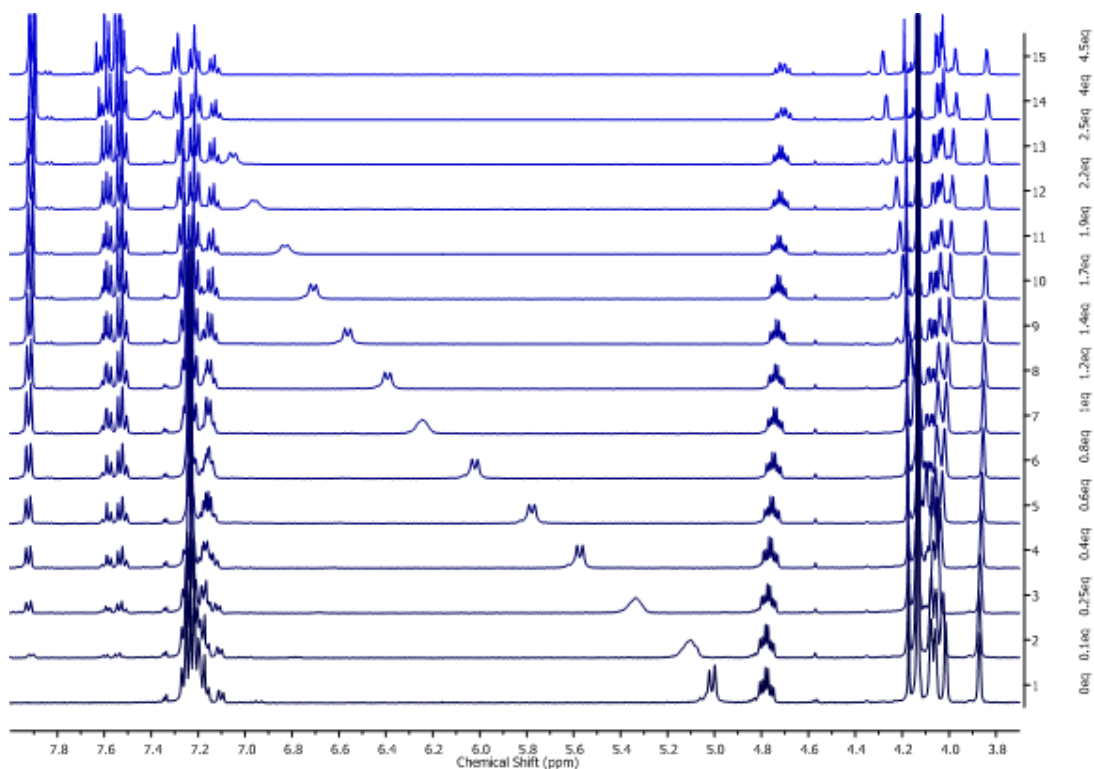


Figure S12 Stacked ^1H NMR Spectra for the titration of **5** (5 mM) with (*S*)-**9** (50 mM) in CD_3CN at rt (addition of up to 6 equivalents).

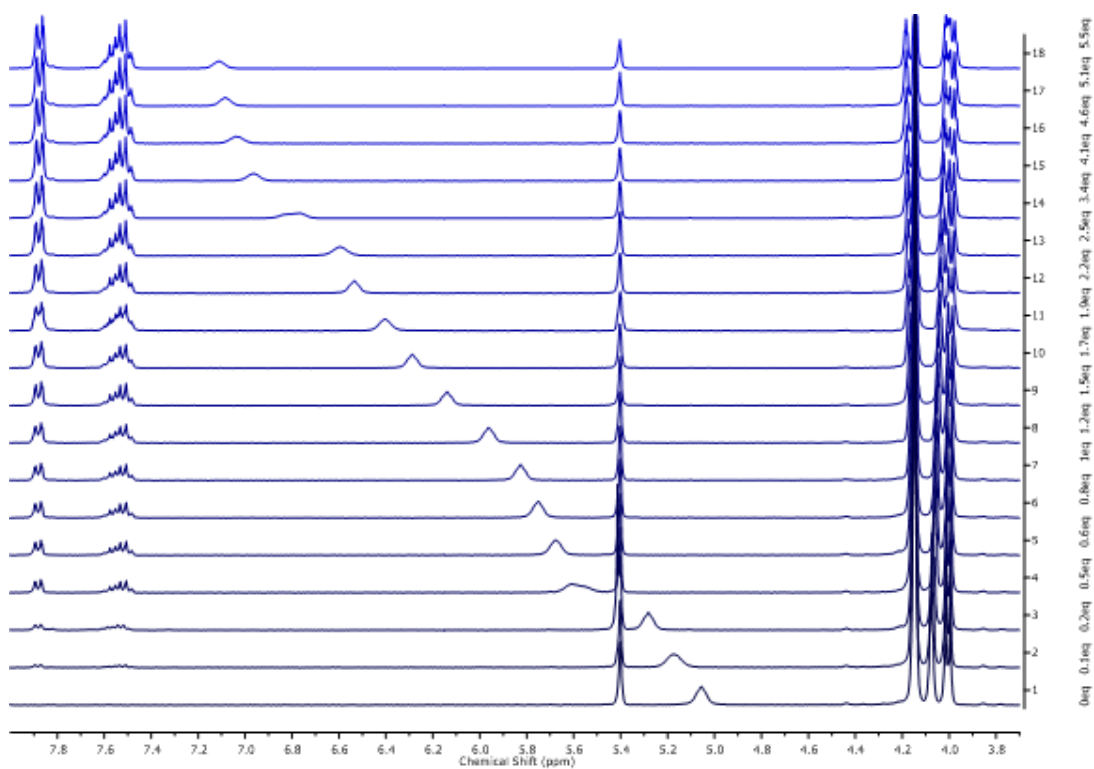


Figure S13 Stacked ^1H NMR Spectra for the titration of **6** (5 mM) with (*R*)-**9** (50 mM) in 2:1 $\text{CD}_3\text{CN}/\text{CD}_2\text{Cl}_2$ at rt (addition of up to 6 equivalents).

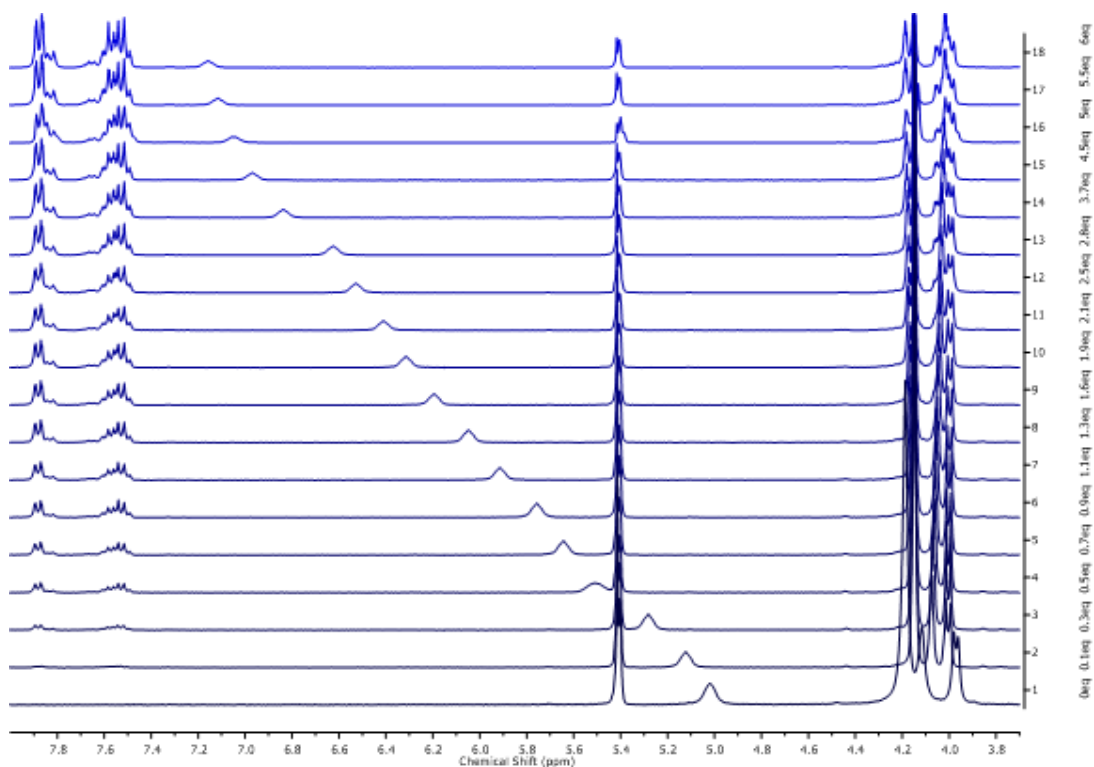
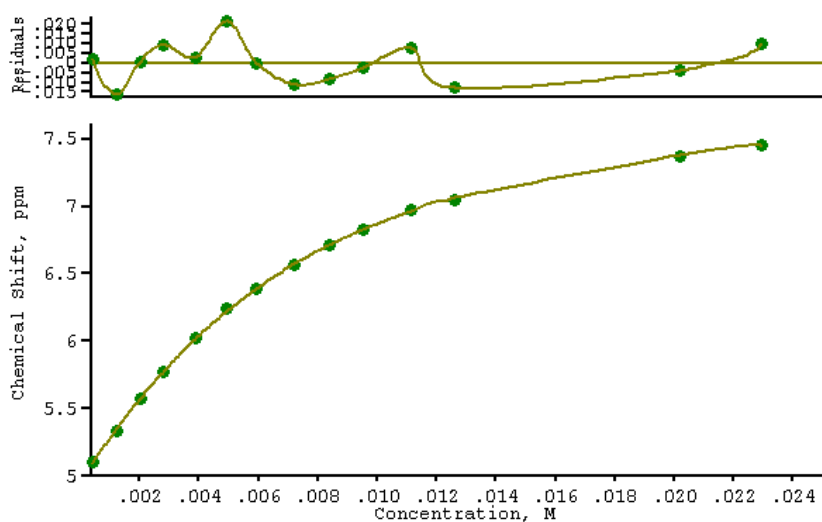


Figure S14 Stacked ^1H NMR Spectra for the titration of **6** (5 mM) with (*S*)-**9** (50 mM) in 2:1 $\text{CD}_3\text{CN}/\text{CD}_2\text{Cl}_2$ at rt (addition of up to 6 equivalents).



Calculations by WinEQNMR2 Version 2.00 by Michael J. Hynes

DATA FOR 1:1 COMPLEX USING CHEMICAL SHIFT (TEST11.FIT)

Reaction: $H + G = HG$

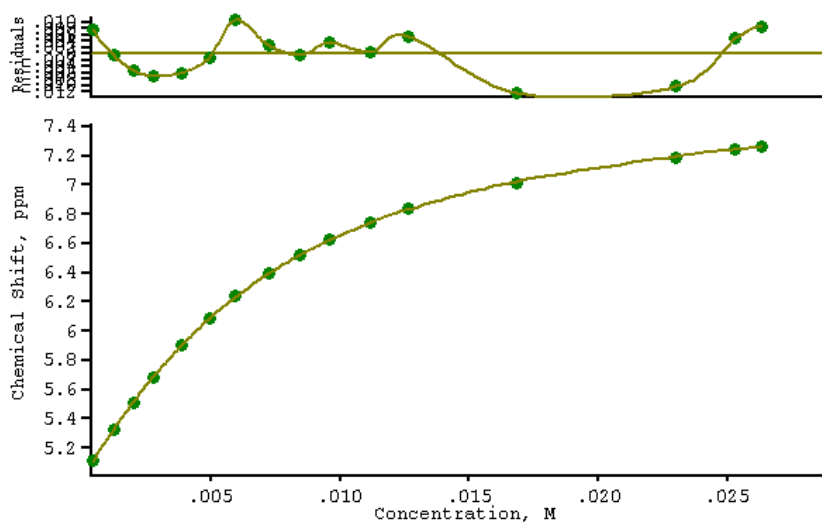
NO.	A	PARAMETER	DELTA	ERROR	CONDITION	DESCRIPTION
1	1	2.58497E+02	2.000E-01	7.124E+00	1.880E+01	K1
2	1	4.96269E+00	2.000E-01	8.434E-03	2.680E+00	SHIFT H
3	1	7.96040E+00	1.000E+00	2.088E-02	1.395E+01	SHIFT HG

0RMS ERROR = 1.11E-02 MAX ERROR = 2.17E-02 AT OBS.NO. 6

RESIDUALS SQUARED = 1.36E-03

RFACTOR = 0.1534 PERCENT

Figure S15 ^1H NMR titration of chiral host **5** with TBA salt of (*S*)-**9** in CD_3CN



Calculations by WinEQNMR2 Version 2.00 by Michael J. Hynes

DATA FOR 1:1 COMPLEX USING CHEMICAL SHIFT (TEST11.FIT)

Reaction: H + G = HG

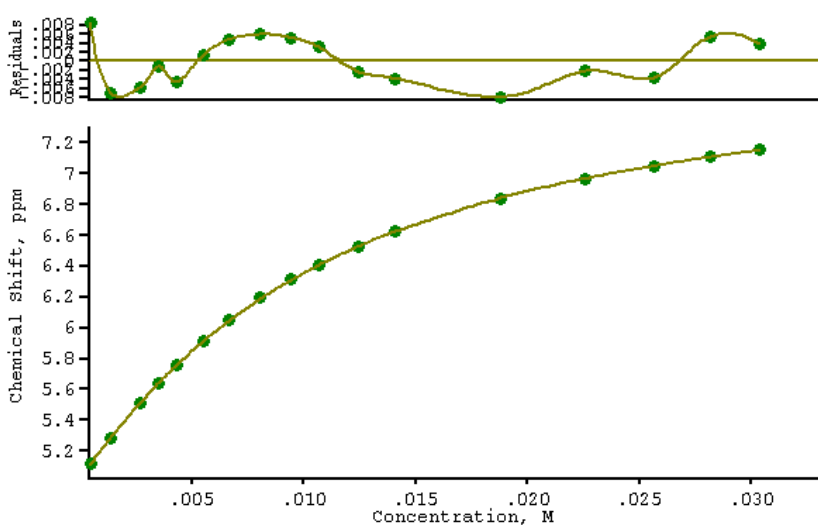
NO.	A	PARAMETER	DELTA	ERROR	CONDITION	DESCRIPTION
1	1	2.17200E+02	2.000E-01	3.509E+00	1.558E+01	K1
2	1	4.98101E+00	2.000E-01	5.585E-03	2.885E+00	SHIFT H
3	1	7.72352E+00	1.000E+00	1.071E-02	1.070E+01	SHIFT HG

ORMS ERROR = 7.31E-03 MAX ERROR = 1.25E-02 AT OBS.NO. 13

RESIDUALS SQUARED = 6.95E-04

RFACTOR = 0.1031 PERCENT

Figure S16 ^1H NMR titration of chiral host **5** with TBA salt of (*R*)-**9** in CD_3CN



Calculations by WinEQNMR2 Version 2.00 by Michael J. Hynes

DATA FOR 1:1 COMPLEX USING CHEMICAL SHIFT (TEST11.FIT)

Reaction: $H + G = HG$

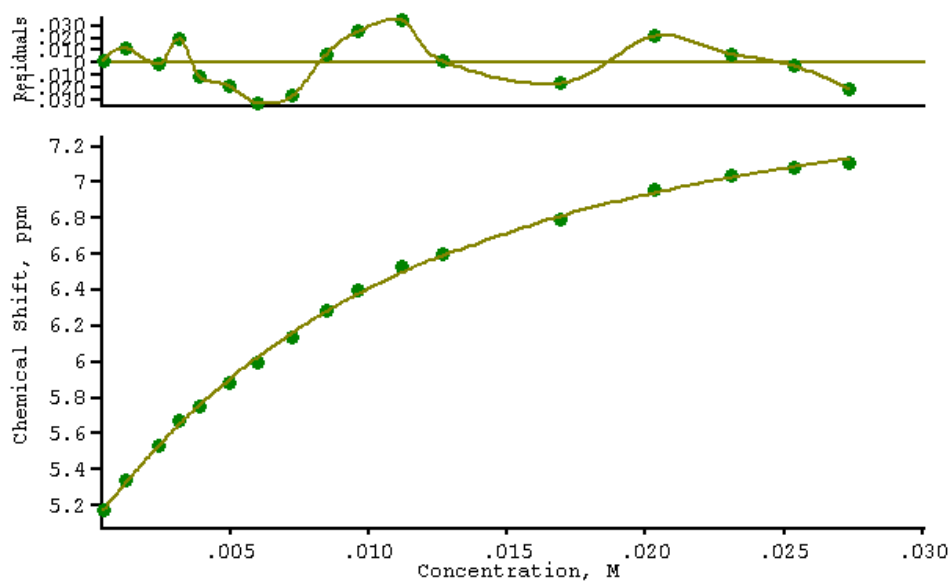
NO.	A	PARAMETER	DELTA	ERROR	CONDITION	DESCRIPTION
1	1	1.20127E+02	2.000E-01	1.654E+00	2.629E+01	K1
2	1	5.01560E+00	2.000E-01	4.222E-03	3.651E+00	SHIFT H
3	1	7.82263E+00	1.000E+00	1.125E-02	1.789E+01	SHIFT HG

0RMS ERROR = 5.47E-03 MAX ERROR = 8.43E-03 AT OBS.NO. 1

RESIDUALS SQUARED = 4.18E-04

RFACTOR = 0.0788 PERCENT

Figure S17 ^1H NMR titration of achiral host **6** with TBA salt of (*S*)-**9** in $\text{CD}_3\text{CN}/\text{CD}_2\text{Cl}_2$ 2:1



Calculations by WinEQNMR2 Version 2.00 by Michael J. Hynes

DATA FOR 1:1 COMPLEX USING CHEMICAL SHIFT (TEST11.FIT)

Reaction: $H + G = HG$

NO.	A	PARAMETER	DELTA	ERROR	CONDITION	DESCRIPTION
1	1	1.21176E+02	2.000E-01	6.718E+00	2.923E+01	K1
2	1	5.08468E+00	2.000E-01	1.534E-02	3.666E+00	SHIFT H
3	1	7.84636E+00	1.000E+00	4.671E-02	2.029E+01	SHIFT HG

ORMS ERROR = 2.04E-02 MAX ERROR = 3.40E-02 AT OBS.NO. 11

RESIDUALS SQUARED = 5.84E-03

RFACTOR = 0.2949 PERCENT

Figure S18 ^1H NMR titration of achiral host **6** with TBA salt of (*R*)-**9** in $\text{CD}_3\text{CN}/\text{CD}_2\text{Cl}_2$ 2:1

4. UV/Vis Binding Studies

UV-Vis measurements were performed using a Cary 5000 spectrophotometer or a Shimadzu UV-1800 spectrophotometer. The receptor (0.025 mM) was titrated with a solution of the guest (6.25 mM) dissolved in the stock solution of the host, to avoid dilution effects. In each titration, the change in absorption intensity was monitored at different wavelengths (between 350 and 410 nm). Binding constants are determined using the Benesi-Hildebrand method. In each titration in DMSO the absorption change is monitored between 365 and 410 nm, and the value of $1/(\Delta A)$ is plotted against the value of $1/[guest]$, giving a value of the binding constant (presented as $\log K$) obtained from the division of the intercept by the gradient, at a specific wavelength. The binding constant was calculated as the average of the ten values obtained from the plots in the wavelengths range, a plot every 5 nm. Each titration was repeated at least once and the experimental error was estimated on the range of $\log K$ values obtained from the different titrations. Representative examples of the titration experiment and the data treatment are shown below in Figures S19 and S20.

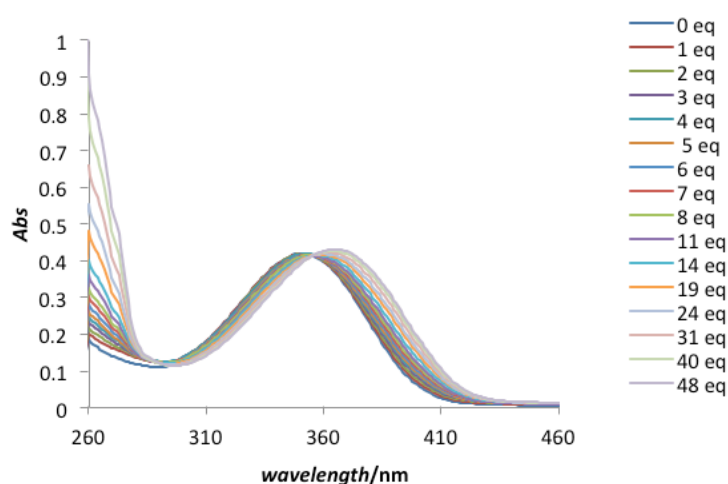


Figure S19 a) UV-Vis titration of **4** (0.025 mM) in DMSO upon addition of (*S*)-**7** at rt; the band at 350 nm decreases and the band at 370 nm increases as the complex forms.

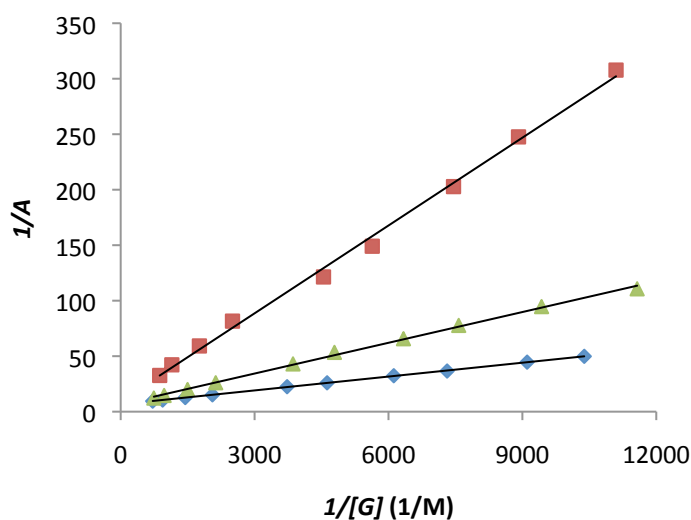


Figure S20 Benesi-Hildebrand plots of **4** (0.025 mM) in DMSO at rt upon addition of (*S*)-**7** (blue diamonds), (*S*)-**8** (red squares) and (*S*)-**9** (green triangles) at 370 nm.

5. Electrochemistry

Electrochemical studies were performed with a BAS 100W electrochemical analyser, with BAS 100W software. All measurements were carried out at 298 K in dry CH_3CN or dry CH_2Cl_2 , in which was dissolved tetrabutylammonium hexafluorophosphate as supporting electrolyte (0.1 M). A conventional 3-electrode system was employed. The working electrode (WE) was a platinum disc electrode (diameter: 1.6 mm, average surface roughness factor recorded equal to 1.7). Silver/silver chloride ($\text{Ag}|\text{AgCl}$) was used as an external reference electrode and a platinum wire was used as auxiliary electrode. Decamethylferrocene, dmfc (0.2-0.8 mM), was used as an internal reference and its redox couple was unaffected by the addition of guests. All cyclic voltammograms were carried out at a scan rate of 100 mV s^{-1} unless otherwise stated. All square wave voltammograms were carried out using a step of 1 mV, with a pulse amplitude of 25 mV and a frequency of 15 Hz. The cells and the volumetric flasks used were cleaned using a 1:1 solution of ammonia and hydrogen peroxide, rinsed 10 times using MilliQ® water (purified with a Millipore Elix-Gradient A10 system, $18 \text{ M}\Omega \text{ cm}$, $\text{toc} \leq 5 \text{ ppb}$, Millipore, France) and dried in the oven overnight. Prior to use, the platinum electrode was polished by hand with aqueous slurries of $0.05 \mu\text{m}$ alumina powder pads and then thoroughly rinsed in deionised water, followed by MeOH, and dried in a directed stream of nitrogen. To check the electrochemical reversibility of the host, voltammetric cycles were performed at different scan rates (100, 300, 500, 700 and 1000 mV^{-1}) between -250 and 700 mV (vs Ag/AgCl). Plots of anodic peak current vs the square root of the scan rate gave a straight line. Half-wave potentials of each receptor, $E_{1/2}$, where $E_{1/2} = (E_p^a + E_p^c)/2$, were independent of scan rate. The receptor (0.5 mM) was titrated with aliquots from a solution of guest (0.05 M) and the shift in the ferrocene-centred redox wave of the receptor monitored. Additions were continued until no further shifts were observed, to ensure that the receptor was fully complexed. Control studies in the absence of the receptors revealed that the guests showed no redox activity in regions where complexation-induced shifts in potential were observed. Titrations were also used to determine any chiral sensing effects. The observed shift in electrode potential was evaluated for the addition of each aliquot of enantiomers and plotted against molar equivalents of guest. Potentials in the text are quoted vs decamethylferrocene (dmfc). $E_{1/2}$ of dmfc is -0.507 V vs. ferrocene in CH_3CN and TBAPF_6 (F. Barrière and W.E. Geiger, *J. Am. Chem. Soc.* 2006, **128**, 3980-9).

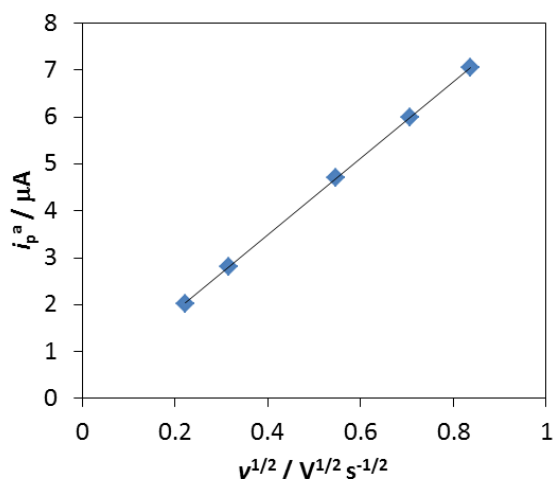


Figure S21 Dependence of anodic peak height (i_p) on the square root of the scan rate (v) for receptor **2** ($5 \times 10^{-4} \text{ M}$ in MeCN, TBAPF_6 0.1 M, with dmfc at rt.).

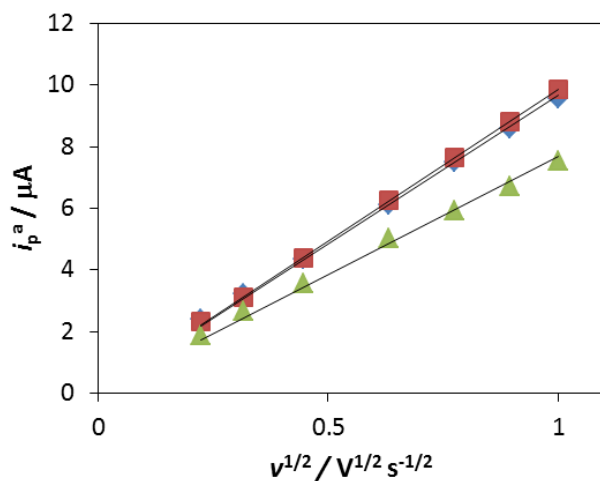


Figure S22 Dependence of anodic peak height (i_p) on the square root of the scan rate (v) for the three 1:1 complexes with receptor **2** (5×10^{-4} M in MeCN, TBAPF₆ 0.1 M, with dmfc at rt.) Diamonds, **2** + (S)-7; squares, **2** + (S)-8 and triangles, **2** + (S)-9.

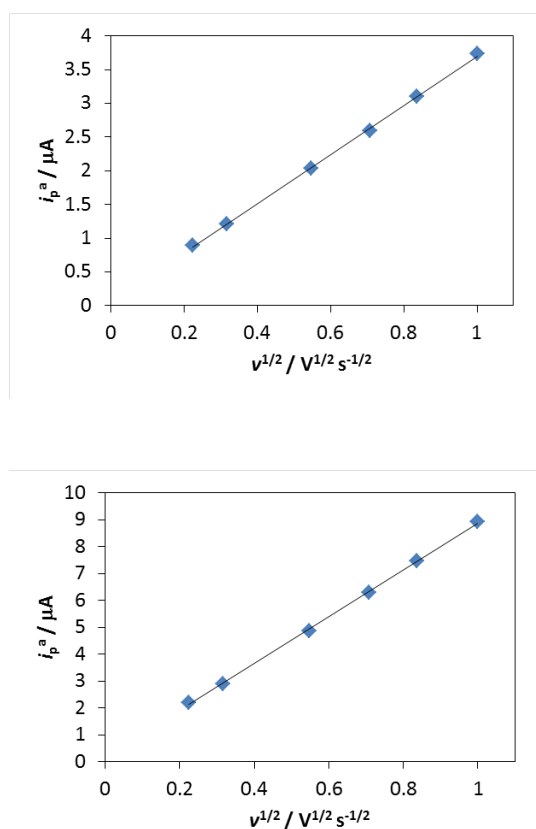


Figure S23 Dependence of anodic peak height (i_p) on the square root of the scan rate (v) for **5** (top) and **6** (bottom) (5×10^{-4} M in MeCN, TBAPF₆ 0.1 M, with dmfc at rt.) (2×10^{-4} M in MeCN, TBAPF₆ 0.1 M, with dmfc at rt.)

Figure S24 below shows the titration curves for the enantiomeric pair of receptors (R_p)-**3** and (S_p)-**3** with the enantiomeric pair of guests (S)- and (R)-**8**. Despite repeated experiments confirming the expected mirrored behaviour, that is, near identical curves for the formation of enantiomeric complexes (e.g. formation of complexes (R_p)-**3**:(R)-**8** and (S_p)-**3**:(S)-**8** give the higher curve in each case), the differences observed are small and in any case are not outside of the confidence limits of the experiment.

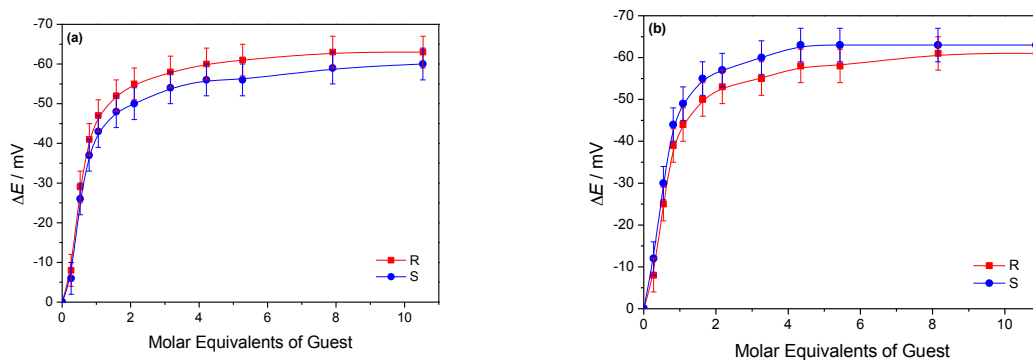


Figure S24 Values of ΔE (mV \pm 4 mV) for receptor (R_p)-**3** (left) and its enantiomer, receptor (S_p)-**3** (right) upon addition of (S)-**8** (red) and (R)-**8** (blue).

Digital Simulations of the voltammetry

Appearance of voltammetry (“one-wave” vs “two-wave” behaviour): The tendency for voltammetry to display “one-wave” behaviour (a gradual shift in $E_{1/2}$ as a host is titrated with a guest) or “two-wave” behaviour (in which a new redox wave starts to appear as that of the host diminishes in height) was examined in some detail by Kaifer *et al.* (ref 23a) who compared experimental data with simulations of voltammetry. In this study, digital simulations of cyclic voltammograms corresponding to cyclic crown ethers with a reducible redox group were performed, in the presence and absence of group I metal cations, which bind to the crown ethers. The study involved an analysis of Equation 1, which relates the redox response to complexation, ΔE , where $\Delta E = E_{\text{HG}}^{\text{ox}} - E_{\text{H}}^{\text{ox}}$, to the ratio of binding constants in the oxidised and reduced forms of the receptor, $K_{\text{ox}}/K_{\text{red}}$:

$$\ln(K_{\text{ox}}/K_{\text{red}}) = -nF(E_{1/2(\text{HG})} - E_{1/2(\text{H})})/RT \quad (\text{Equation 1})$$

From these simulations, Kaifer and co-workers found that the observation of two-wave or one-wave behaviour was strongly dependent on the strength of the host-guest binding interaction in the neutral redox state (in their studies, this was K_{ox} , which could be measured independently) and on the ratio of the binding constants in the reduced and oxidised forms (which affects the shift ΔE). Two-wave behaviour was observed for binding constants of $>10^4$ in the neutral redox state (and with a ratio of binding constants of 10,000). In our studies, the binding constants in MeCN (used for the electrochemistry) would be expected to be significantly greater than those calculated in DMSO (Table 1 of main text: values were *ca* 10^3), which would make the observation of two-wave behaviour in some of our voltammograms feasible. We might expect to see two-wave behaviour for complexes with large changes in binding constant upon oxidation and with large binding constants in the reduced form (K_{red}). Out of the three guests studied with receptor **2**, that which binds most weakly, mandelate **8**, is the only one that induces one-wave behaviour, an observation in keeping with the idea that lower binding constants are more likely to be associated with one-wave behaviour. However, receptor **1**, which generally exhibits higher binding affinities with the guests than receptor **2**, always exhibits predominantly one-wave behaviour with all three guests (observed when adding sub-stoichiometric amounts of guest). Whilst the shift in potential, and hence the difference in position between peaks corresponding to complexed and uncomplexed receptors, obviously influences our ability to discern two peaks, the relative peak heights will also have a bearing on their resolution. One factor not included in the treatment by Kaifer *et al.* was the possibility of a change in diffusivity, which will affect the peak height. In Kaifer’s work, it was assumed that the diffusivities of all the species (oxidised and reduced forms of both host and host-guest complex) were equal. In their study, crown ether-metal complexes were investigated and so a change in shape and thus large variation in diffusivity was unlikely. In our case, however, it is conceivable that the host-guest complex could be significantly larger than the host alone, resulting in lower diffusivity. This could result in a smaller contribution of the HG redox peaks to the overall voltammogram and an appearance of one, perhaps broader peak. To investigate this idea, we simulated voltammograms of the interactions between receptors **1** and **2** with guests (*R*)-**9** and (*S*)-**9** using the package Digisim. The values of diffusivity were obtained from the CVs, plotting i_p^a as a function of potential scan rate and using the Randles-Sevcik equation. Values of diffusivity for receptor **1** fall almost by a factor of 2 on complexation, whereas for receptor **2** (containing an extra methyl group), the values fall by only *ca* 10%. The experimental and simulated CVs are presented in Figure S25. It should be noted that the one-wave vs two-wave behaviour is more apparent in SWV but CV data are provided for ease of comparison.

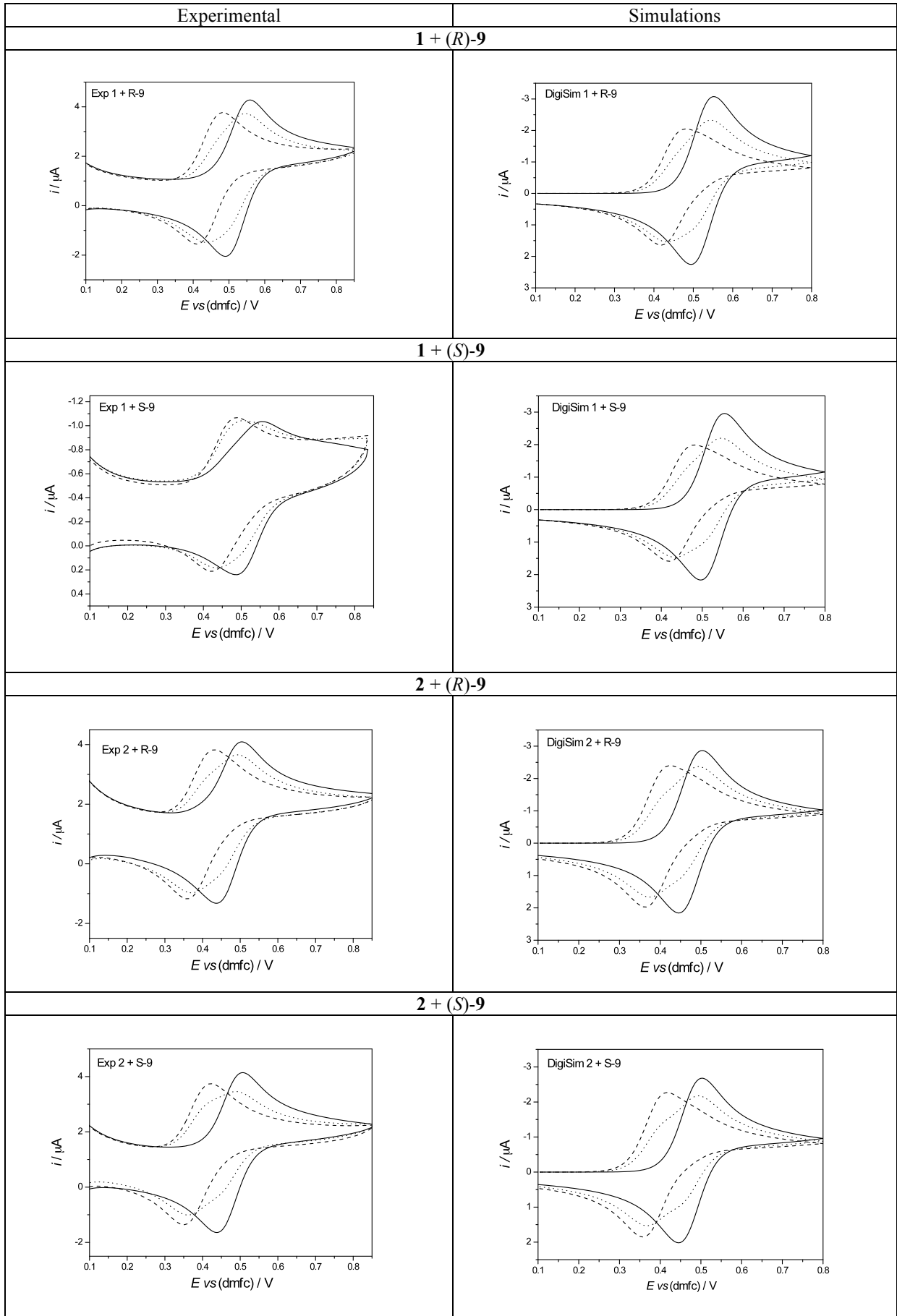


Figure S25 Experimental (left) and simulated (right) cyclic voltammograms for receptors **1** and **2** upon addition of (*R*)- and (*S*)-**9**. Plain line, 0 equivalents; dotted line, 0.5 equivalents, dashed line, 1.0 equivalents

Comparing complexes of similar binding affinity and differing total potential shift (Table 1 in main text), one-wave behaviour is more pronounced for **1**+(*R*)-**9**, of smaller potential shift, compared to **2**+(*S*)-**9**, which has a larger potential shift. These findings are in keeping with the conclusions drawn by Kaifer *et al.* However, if we now compare the behaviour of **1**+(*S*)-**9** and **2**+(*R*)-**9**, which have similar total potential shifts, the more weakly binding system (**2**+(*R*)-**9**) appears to have more two-wave character (this effect is more noticeable by SWV), which is not explained by the conclusions of Kaifer *et al.* Hence, we suggest that it is important to take into account differences in diffusivity between host and host-guest complex when simulating voltammetry for systems where a significant change in size can be expected upon complexation.

Conditions and parameters: The concentration (0.5 mM), initial potential (Table 2), final potential (Table 3), scan rate (0.1 V s⁻¹), WE radius (0.08 cm) and temperature (293 K) were the same as in the voltammetric experiments. A binding constant value needed to be estimated for the simulation to fit the experimental data in MeCN, in which a near full shift was observed upon the addition of one molar equivalent of guest at 0.5 mM. It was found that a satisfactory fit could be achieved by multiplying the appropriate binding constants in DMSO (Table 1) by 100. The diffusion coefficient, D ,²⁰ was calculated in each case by plotting i_p values for the oxidised and reduced forms against the square root of the scan rate and using the Randles-Sevcik equation.²¹ An error of $\pm 1.5 \times 10^{-6}$ was estimated from the experimental data for the free host.